Machine learning approach for weld configuration classification within the GTAW process

Theo Boutin, Issam Bendaoud, Josselin Delmas, Damien Borel, Cyril Bordreuil

CIRP Journal of Manufacturing Science and Technology 47 (2023) 116–131

Contents lists available at ScienceDirect

CIRP Journal of Manufacturing Science and Technology

journal homepage: www.elsevier.com/locate/cirpj

Full length article

Machine learning approach for weld configuration classification within the GTAW process

Theo Boutin [a,b,*], Issam Bendaoud [b], Josselin Delmas [a], Damien Borel [a], Cyril Bordreuil [b]

[a] EDF R&D, 6 Quai Watier, Chatou, 78400, France
[b] LMGC University of Montpellier, Montpellier, 34000, France

ARTICLE INFO

Keywords:
GTAW welding
Instrumentation
Machine learning
Image processing
Welding physics

ABSTRACT

In the present study, an attempt has been made to couple experimental data with a machine learning (ML) approach to classify several weld configurations. An ML model has been developed and fed into experimental data captured by several sensors during the gas tungsten arc welding (GTAW) process. On the one hand, welding parameters (voltage, current, wire speed, welding speed, etc.) were used to monitor the control energy transmitted during welding. On the other hand, cameras coupled to an image-processing algorithm were employed to capture the weld pool contour in situ. A database was also constructed to store, label, and order the obtained information. This database was then used for the various training, validation, and prediction steps of the ML model. The welding configurations were then classified using a KNN classification algorithm, which was then analyzed for their efficiency (accuracy, processing time, etc.). It was shown that image processing combined with ML can be trained with the features which were extracted to predict the classification of welding configurations. The ultimate perspective of the current study is to realize real-time identification and modification of welding operating conditions.

Introduction

For many years, welding metals by arc welding processes such as gas tungsten arc welding (GTAW) and gas metal arc welding (GMAW) in which the metal is melted has been one of the most commonly used joining techniques for steels including stainless steels in many industries, such as energy, aerospace, petrochemical, civil engineering, and so on [4,13–16]. The GTAW technique requires a heat source of sufficient intensity to melt the material and ensure the continuity of the welded parts. The Tungsten Inert Gas (TIG) welding process produces high quality welds due to the fact that the arc is created without metal transfer, resulting in exceptional stability. However, the intense radiation from the arc makes it difficult to visualize, and the welding energy (plasma density) determines the spectral nature of the arc, complicating matters [10]. Any welded joint must provide optimal safety and endurance under service conditions to guarantee the desired level of joint safety (the weld must be of high quality). In an industrial context, the robustness of installed components must be guaranteed. Like, a multi-pass butt joint may contain various defects in both its surface (cracks) and volume (lack of penetration, fusion), as depicted schematically in Fig. 1. These defects can negatively affect component assembly. The quality of such assemblies is checked post-construction by non-destructive examination (X-rays, ultrasound, penetrant testing, etc.). In order to guarantee the quality of a welded joint, the welding process must meet specific standards, and in certain situations must adhere to prescribed building codes and regulations. The welding process must also be carried out under certain conditions and constraints. A welding procedure qualification (PQR) is carried out by the realization of a preliminary welding procedure specification (WPS).

The realization of a QPR by an operator requires them to have sufficient knowledge of the implementation of the inspection method and the capacity to interpret the results obtained. Secondly, the tests require a substantial amount of equipment, are technically costly, and have significant financial consequences if defects are detected. Moreover, in the event of assembly non-conformity, the weld may be repaired (under certain conditions or constraints), thus delaying the manufacturing operation, or may need to be scrapped altogether if the defect is too important.

Several types of disturbance can occur during the welding process, affecting the resulting weld quality. Due to complex multi-physical problems, many phenomena can intervene in a coupled way [9]. It is important to understand and apprehend the various interactions of the physical phenomena involved. An online weld monitoring system capable of detecting instabilities affecting weld quality and even supervising the whole system to prevent these possible defects from occurring

* Corresponding author at: EDF R&D, 6 Quai Watier, Chatou, 78400, France.
E-mail address: theo.boutin@edf.fr (T. Boutin).

https://doi.org/10.1016/j.cirpj.2023.09.006

Available online 10 October 2023

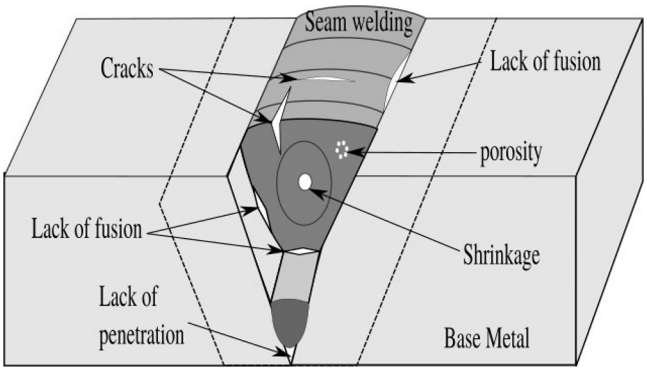

Fig. 1. Schematic presentation of weld defects.

would be a great asset. Numerous experimental methods to ensure in situ control of the welding operation exist in the literature. Various measuring techniques exist, such as [11] use spectroscopic analysis of the arc emission, [19] used acoustic analysis to measure pressure variations due to the arc, and [8] measured melt geometry.

First, [11] proposed a method for automatic detection and classification of welding defects based on the combined use of several machine learning (ML) algorithms, linking arc physics and weld pool behavior in real time based on spectrometry measurements. These authors calculated the plasma electronic temperature using algorithms for quality evaluation and monitored defects in the weld bead such as oxidation due to insufficient shielding gas flow, changes in penetration caused by fluctuations in the welding current source, and thermal distribution. [12] have also developed a photodiode-based system to detect weld defects. Thus, they have shown that photodiode sensors can be an alternative means of spectrometers for welding quality control. In addition, [19] used ML with different decision algorithms (Naive Bayes, Support Vector Machines, Artificial Neural Network) to ensure the quality of shielded metal arc welding (SMAW) operation and to classify the different penetration states. In these latter studies, the melting failures or excess penetration were related to the arc pressure variations during the process, measured through a microphone. However, no processing of the raw signals was performed, nor is any information given on the structure of the database used to feed the ML models. Furthermore, the choice of hyperparameters is not given. [18] use the same input data as the previous study to compare the performance of two new classification models (Decision Tree, Random Forest). For both studies, the Random Forest model showed the best accuracy. In general, the quality of arc welding is mainly a function of weld-pool stability, which depends on the welding parameters and the weldability of the material. So, [8] developed an algorithm for detecting the GTAW weld-pool geometry in real time with image processing methods. Also, these authors implemented an adaptive control system (based on power) to keep the shape and size of the weld pool constant. However, this model is difficult to implement as it requires one model per configuration. [23] has developed a predictive control system to control the welding process based on the dynamic fuzzy model in order to overcome the effects of non-linearity between the model inputs and output. This model is fed by images acquired through a camera placed for the observation of the upper field. All these experiments are carried out in academic conditions (single pass). The transposition to industrial conditions raised different questions. First, the industrial environment is harsh, and second, an adequate database is required which to feed to model. Finally, the most adaptive ML algorithms are needed.

[3] introduced the various artificial intelligence methods in this book. Machine Learning techniques generally fall into two categories: (i) Supervised learning, which consists of labeling a training dataset, provides input values and the corresponding output value to the observation. This type of ML can be used for both classification [18] and regression [21]. (ii) Unsupervised learning has no training data set, and therefore the ML algorithm tries to automatically separate the training data into different clusters attached to a label. Researchers have frequently used ML methods such as [22] developed support vector machine model, [7] used a random forest algorithm, [6] used a k-nearest neighbor model, and finally [17] developed decision tree algorithm to predict the welding state. Also, each ML model has hyperparameters specific to the algorithm used. [2] described these hyper-parameters associated to the model used. Adjusting these hyperparameters can improve model performance. Furthermore, researchers have started to introduce the use of deep learning such as convolutional neural networks (CNNs) for image analysis to monitor the welding process. [1] used CNNs to classify defects in tungsten inert gas (TIG) welding. Finally, [5] records and merges data from multiple sensors provides a wealth of information that is highly useful for fault detection; this implies the fusion of multi-sensor monitoring data and welding processes control.

The objective of the current study is to implement a robust ML algorithm in the monitoring and classification of GTAW welding procedures on 316L stainless steel and filler metal, using several sensors non-intrusive and embedded in the welding torch (voltage, current, wire-feed speed, shielding gas, cameras) in order to use it on a large scale. To optimize solutions applicable in an industrial setting, it is essential to observe the weld pool behavior on the electric arc side in-situ. This ensures that the precise amount of material is added for controlling the welding operation's quality. All the sensors must be non-intrusive and mounted on the welding torch. First the materials and methods were described. The applications considered can involve long manufacturing times, which implies a massive flow of data to be processed and stored, which may itself lead to longer processing times. And then it was described how a database was constructed and used to train the algorithms according to the particular objective or defect search. In addition, a preliminary data-processing step permits classification of an operating mode from physical data (e.g. melt pool geometry), which allows data reduction and time-saving during the training of the ML algorithms. Finally, the last part of the work consists of testing the ML algorithm on experimental data, allowing us to predict and classify the operating modes and validate the global approach.

Materials and methods

Experimental setup

In this section, the experimental platform for the test procedure which was used in the current study is presented. To visualize the in situ weld-pool behavior, several measuring devices were chosen to meet the requirements and to allow observation of the weld pool in situ as depicted schematically in Fig. 2. On the one hand, arc welding is governed by the electric current (I), welding voltage (U), welding speed (Vs), wire speed (Vf), and shielding gas, ensuring operation quality and directly influencing the residual weld-pool condition. A change or fluctuation of this energy affects the dynamic weld-pool behavior. Monitoring these parameters during the operation is therefore essential (Fig. 2). Acquisition of process parameters (voltage, current, etc.) is carried out continuously. On the other hand, to follow the evolution of the weld-pool stability, it is necessary to capture visual data using cameras (global field). Using these sensors makes it possible to locate fluctuations in weld-pool behavior during the manufacturing process that could affect assembly integrity. Also, certain constraints must be taken into account, such as size, weight, and accessibility. Finally, synchronization of the acquisition chain from the different sensors must be guaranteed to allow coupling between the different measuring devices.

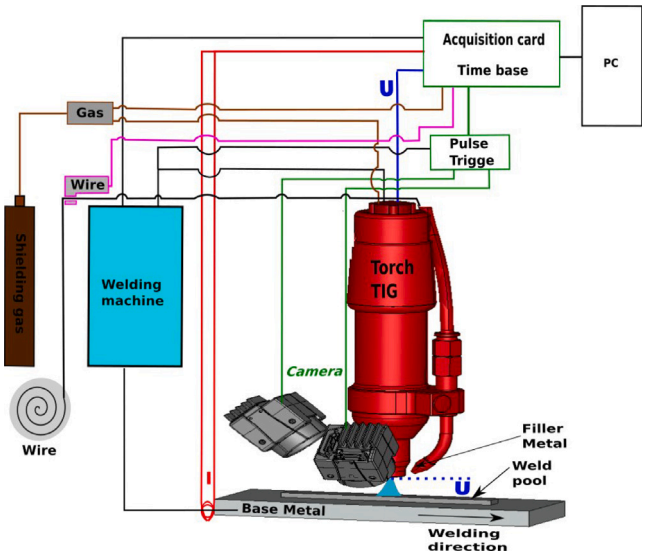

(a)

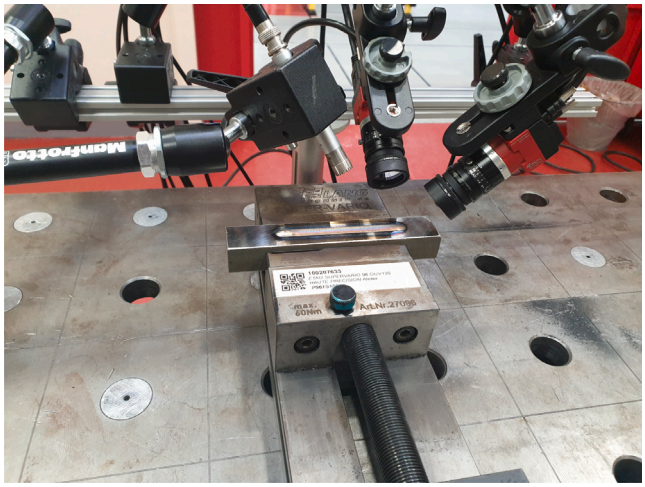

(b)

Fig. 2. (a) Sensors diagram and installation, (b) camera positions.

Welding process

In this section, the welding procedure is presented (metal base geometry). This test campaign was carried out on 316L austenitic stainless steel sheets with dimensions of 150 mm × 50 mm × 10 mm with a metal input of the same material to create the weld. This geometry allows us to overcome the problem of distortion of the part, and lowers the potential for penetration of the weld pool through the material, which would require protection on the back side. The installation of various sensors made it possible to follow the weld-pool evolution and to ensure a fixed set of process parameters during the GTAW welding operation.

In situ measurement of the welding process

In this section, the sensors used to measure the process parameters are presented (Fig. 2). These controlled parameters (more commonly referred to as heat input or linear energy (Eq. (1)) directly affect the energy transmitted to the workpiece and modified weld pool shape. The presence of the electric arc during welding, which is extremely radiant, also induces multiple disturbances (electromagnetic, electrostatic, magnetic noise, etc.). These disturbances can alter the measurements taken during the acquisition chain (sensor, conditioner, sampler etc.) and necessitate specific devices to compensate for this noise (faraday cage, twisted wires, shielding twisted wires, etc.). [20] shows the different ways to protect the measures.

$$E = \frac{U\,I}{W_s} \tag{1}$$

With E: heat input (J/mm), U: voltage (V), I: current (A), and W_s: welding speed (mm/s). In order to control the power of the electric arc during the welding process, electrical parameters (voltage and current) are acquired continuously, which are used to estimate the difference between the power delivered by the generator and the instruction. First, the voltage is measured as close as possible to the arc between the electrode and the workpiece. Second, the current is measured with a LEM Hall effect sensor (reference: LF 510-S). In addition, sensors used to measure the gas protection flow and the wire speed. The wire speed is measured using an HKS-Prozesstechnik sensor (reference: DV25M). This measurement provides information on the material input into the weld pool, which can influence its geometry, and this information is used to control the regularity with which wire is fed into the weld pool. The gas flow is a parameter that is not to be neglected because it ensures protection against oxidation of the molten metal, bead quality, good weld pool wettability, and arc stability. This measurement is obtained with an HKS sensor (reference: GM30L10B-S3). Finally, these process parameter measurements guarantee the repeatability of the tests. The process parameters are acquired at a frequency of 1000 Hz.

Camera capabilities

In this section, the experimental device used to follow the evolution of the weld pool dynamics is presented. Thanks to the flat fusion line configuration with filler metal without space, two Alvium U-051 cameras encoded in 12 bits (Fig. 2) can be installed allowing top face observation (weld pool oscillation and width) and side face observation (weld pool height, wetting, filler metal arrival into the weld pool) simultaneously. The use of two fields of view increases the amount of visual information obtains on the appearance of the weld pool, which in turn allows better quality control during the welding process. Due to the obstructing presence of the torch, it is not possible to position cameras perpendicular to the molten pool, and so these are mounted on articulated arms to allow them to be positioned precisely. The filters used are narrow-band (10 nm) interference filters centered on the selected wavelengths. In addition, the cameras are equipped with a 50 mm focal length lens. A 980 nm band-pass filter is used with an 8/f aperture for the top-facing view, and a 950 nm band-pass filter is used with an 8/f aperture for the side-facing view. Finally, the resolutions are 524 × 724 pxls with an exposure time of 176μs. In some cases, an increase in exposure time can blur the image. However, in this case, the images obtained are clean and clear. Finally, the cameras have an acquisition frequency of 50 Hz.

Measurement synchronization

All observation data are collected by a central data acquisition system (personal computer (PC)). The PC is connected to a Labjack T7-type acquisition card which allows the observations to be synchronized with each other. In addition, an Arduino Mega card is also connected to the computer, which is used to control the camera pulse (acquisition frequency). Finally, due to different sampling frequencies between the sensors or different characteristic times, the development of this acquisition unit is necessary to allow the coupling between the different measurement means in order to increase the range of observable phenomena during a welding operation (see Fig. 3).

Raw data structure

Experimental approach for optimal data analysis

Knowledge of the weld-pool behavior during the welding process is essential for understanding the physical mechanisms (weld-pool dynamics, convective motion, etc.) taking place therein. The information obtained is essential for in situ quality control of the weld pool.

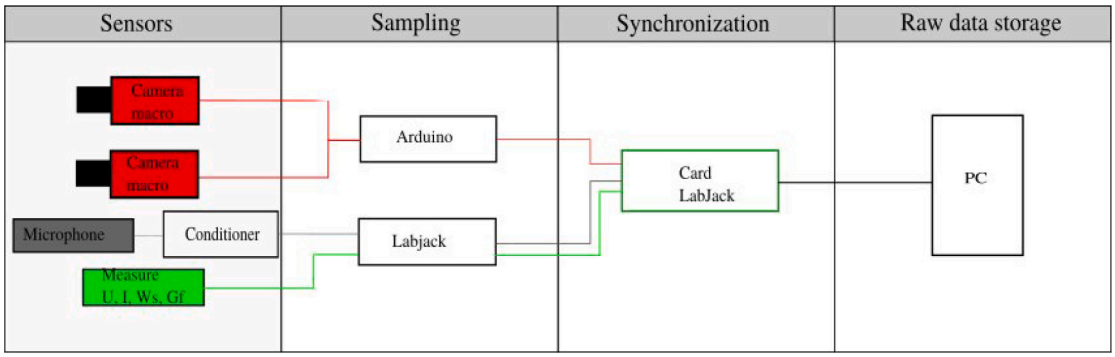

Fig. 3. Principle of an acquisition chain.

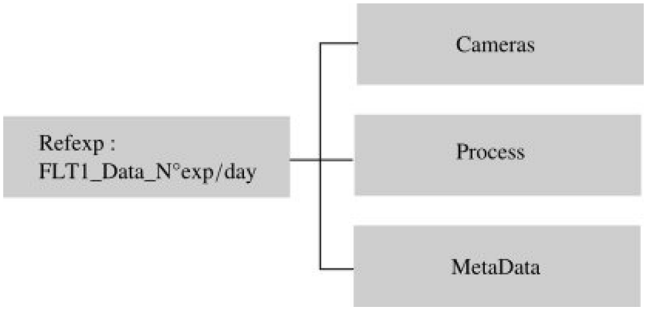

Fig. 4. Global architecture to database.

The experimental facilities (welding robot, different sensors introduced around the operation, and acquisition software) allow us to collect a large amount of data from the different experimental runs. In this section, the database implementation that allows us to optimize data collection from all the different experimental runs is present and the processing pipeline used to process the information coming from the sensors for the analysis of a welding operation.

Data structure and traceability

In this section, the hierarchical structure of our experiments is described, which remains the same regardless of the type of process under analysis or the operating mode used. In addition, each file or subset of files is initialized upon onset of an experimental run, allowing experimental database management, and these files are saved as soon as data acquisition has been stopped.

Two methods were used to make it possible to return to any given moment of data capture during the different experimental runs. The first consists in setting up a metadata file (of XML type). This file stores the information related to the operating parameters governed by the welding operation qualification standard (voltage, intensity, etc.), in addition to the date, the names of the operators, and information of various other types. In this way, each experiment has an "identity card" by which it can be identified. This format is advantageous because of its simplicity of use, its flexibility, its relatively simple architecture, and its extension possibilities. The second method consists in using acronyms in the experiment study. The first letters of each word of the current study (e.g., FLT1, which stands for Fusion Line TIG number 1), coupled with the date on which the experiment was carried out, and finally the current experiment number on that day (FLT1_200421_03 ": Fusion Line TIG performed on April 20, 2021; third test run of the day).

Different techniques exist in the literature to ensure fast and automatic reading of the different data types present in this database. Solutions considered advantageous in this setting are those that incorporate a file format that is intended mainly to store multidimensional tables of numbers and therefore scientific data. In addition, file compression is an asset for economizing storage space. For reasons of ease of data automation development, the HDF5 format is chosed for our study. Furthermore, to allow efficient reading, the storage structure is designed to be similar between experiments. Fig. 4 presents the data hierarchy, which mainly includes the data from the measuring instruments presented in the previous section. There are two important elements to the hierarchy: A metadata file is attached in the header of each folder, allowing automation of the reading process of data coming from the sensors during the various operating modes. Secondly, there is a folder for every type of physical quantity.

Experiment analysis

In this section, an example analysis of the data from a particular experimental run is presented with the aim of showing the importance of both signal synchronization and consistency in the structure of information prioritization. A TIG weld was carried out and monitored as above with the objective of analyzing the evolution of the weld pool geometry during operation without variation of the welding parameters (voltage, current, wire feed rate, gas flow). The process parameters used are illustrated in Table 1.

During this experiment, the current, voltage, wire feed rate, and gas flow were measured, and to follow weld-pool evolution, two cameras were installed as described above (cf. Fig. 2). The acquisition frequency for the process parameters is 1 kHz in each of the inputs on the labjack card and the acquisition frequency for the cameras is 50 Hz.

Fig. 5 shows an example of synchronized test results. First, this shows how the process parameters are monitored continuously, allowing us to ensure the process parameters fixed on the welding generator. For a set current of 150 A, a current of 143 A is measured. Also shown are the two field views obtained through the cameras. Here, two time points have been chosen to visualize the process parameters at those two points during image capture. As the sensors capture information at a different rate from our sampling frequency, it is of primary importance to ensure synchronization between the different sensors.

Data collection

Many types of information can be extracted from these images, such as weld-pool size, and the consistency with which metal is delivered to the weld pool and its influence on its final shape, which are related to the process parameters. These different quantities of interest are necessary in order to study and understand the physical phenomena. A contour-detection algorithm was used in conjunction with these images to estimate the geometry of the weld pool based on the different studies seen in the literature.

Understanding the physical mechanisms acting in the weld pool and their influence on its behavior is of utmost importance for ensuring the quality control of welded joints. Furthermore, the behavior of the

Table 1
GTAW welding process parameters.

Experiment	Intensity (A)	Voltage (V)	Welding speed (m/min)	*E* (J/mm)	Wire feed rate (m/min)	Gas flow rate (L/min)
FLT1_200421_03	150	11.8	0.15	708	3.0	13.0

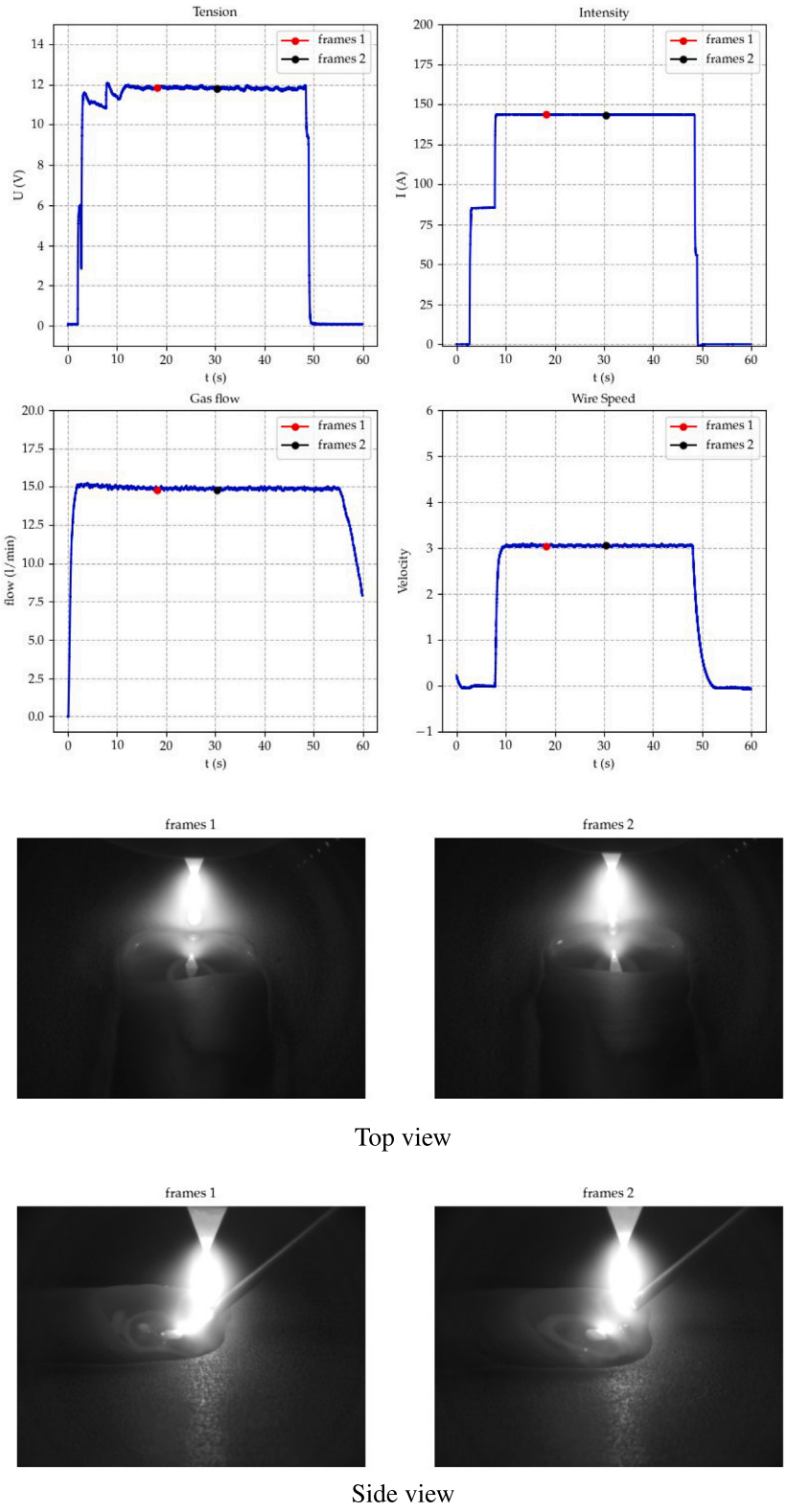

Fig. 5. Images and signals synchronized parameters for campaign analysis.

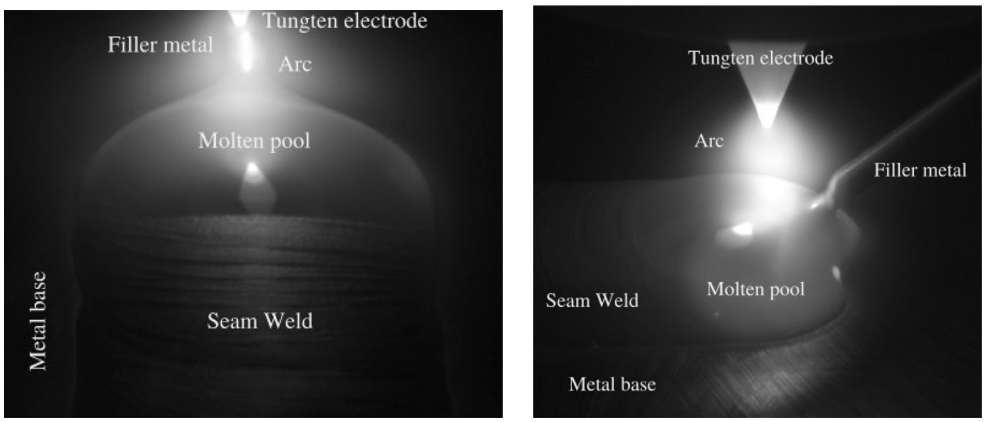

Fig. 6. (a) Example of an image acquired from above the weld. (b) Example of an image acquired from the side.

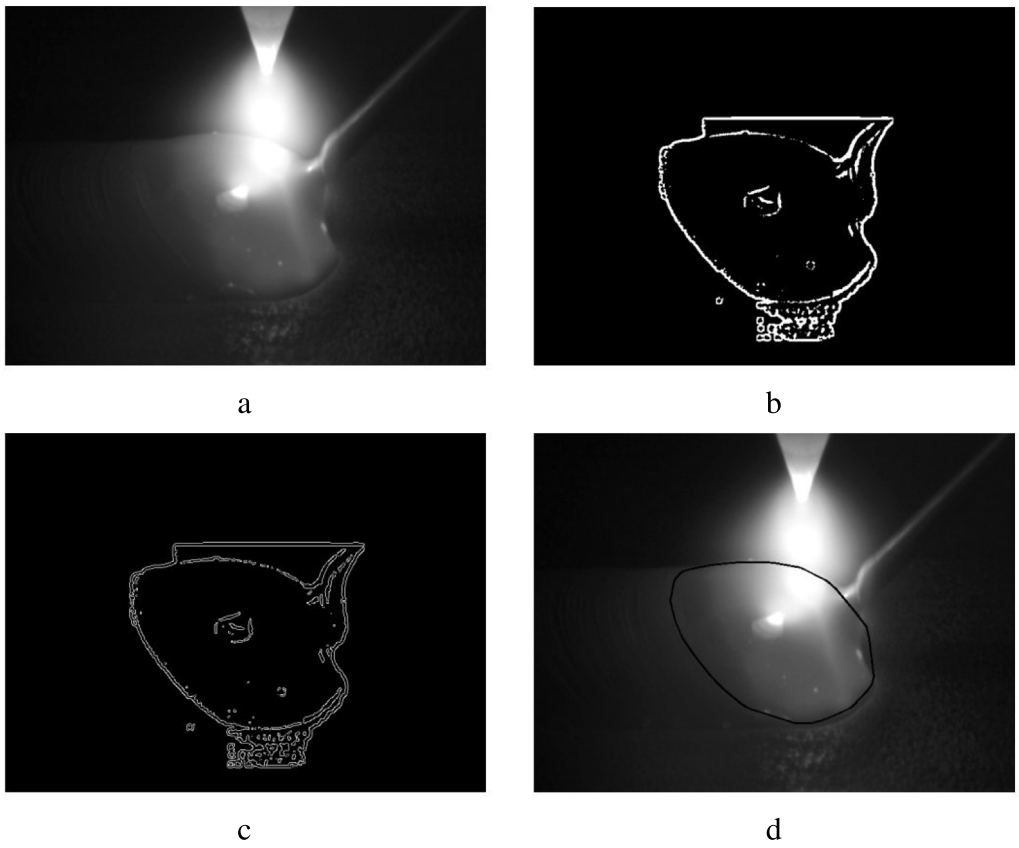

Fig. 7. (a) Image rectification via a calibration test pattern. (b) Use of an adaptive threshold filter. (c) Use of a Canny filter. (d) Edge detection using the α-shape method coupled with a graph algorithm.

wetting liquid metal is directly related to the base metal spreading. Together, these factors contribute to the geometry of the weld pool, directly influencing the quality of the final joint. Observation of the welding process and real-time analysis of the interactions between the different interfaces is therefore a major asset in ensuring the integrity of the welding operation.

Imaging the weld pool during GTAW

First, the choice of filters is essential for masking the electric arc and its radiation (cf. Section "Camera capabilities"). Second, a standard experiment is carried out to confirm the chosen camera parameters, such as exposure time and camera orientation for the desired field of vision. In addition, the various image-processing operations are optimized in order to ensure we obtain the maximum amount of information related to the geometry of the weld pool. Also, to minimize modifications between different test runs and to guarantee repeatability, exposure times, filters, and camera positions were chosen with precision and are similar from one experiment to another. Fig. 6 shows the top and side-view images of the weld pool from which parameters related to its geometry can be obtained.

The area of the weld pool mainly depends on the heat input, and once the weld pool is in the quasi-stationary zone, it should maintain a

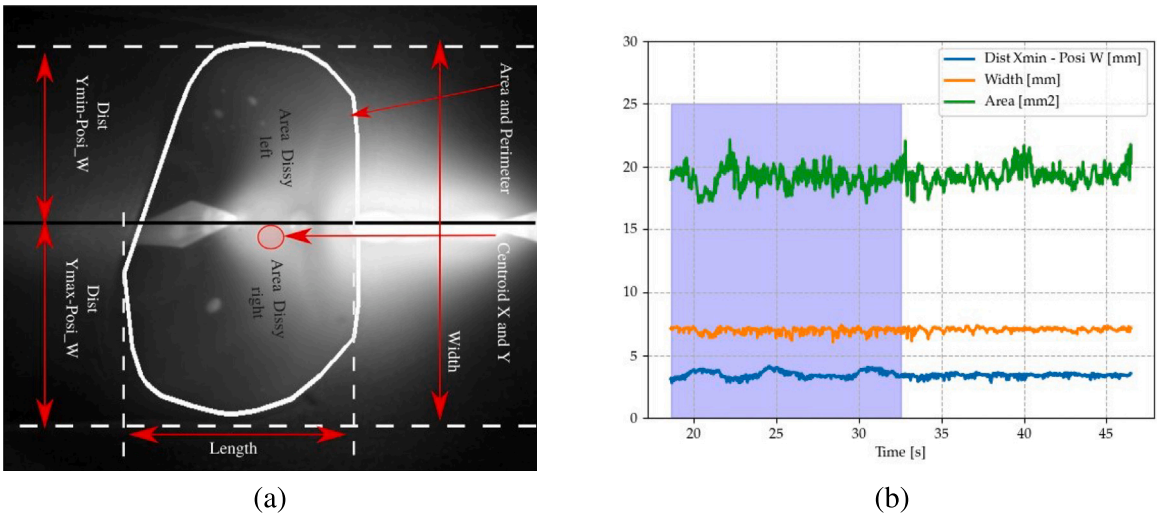

Fig. 8. (a) Weld pool features extraction. (b) Example of geometric characteristics extracted from the weld pool contour: DistXmin - Posi W has instability while keeping the area and a bounding box constant.

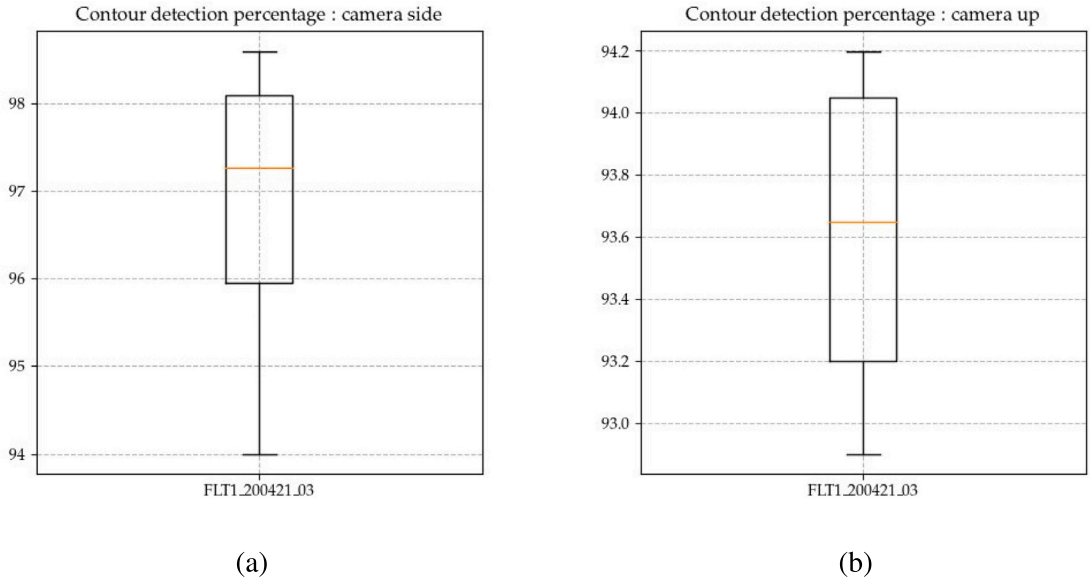

Fig. 9. Percentage of edge detection for both fields of view: (a) Side view; (b) Top view.

constant geometry. In addition, the area can provide information about the weld pool fluctuation (poor weld pool metal behavior due to too much filler metal input compared to the parameterized heat input). These different geometry characteristics can be subject to potential variation during an operation.

Extraction of weld-pool image features

The weld-pool image processing for both fields of view is illustrated in Fig. 7. The first step is to rectify the image warp in order to obtain the actual geometry values during image processing (Section "Camera capabilities"). A region of interest is then chosen according to the position of the weld pool in the image acquired by the cameras. A Gaussian smoothing method is then used to reduce the noise in the image. As the weld pool gray level is different from the base metal, adaptive thresholding is then performed on the area of interest allowing the thresholding to be done dynamically on the image which limits lighting effects. Also, an algorithm is used to detect the edges of the weld pool allowing this particular part of the image to be extracted. As part of this process, the algorithm splits the image into segments and uses an alpha shape object to find all the contours present on the image. Finally, graph theory is used to extract the contour present on the image.

In this paper, different geometric features have been extracted by image processing algorithms such as bounding box (width, length), area, and other features, as illustrated in Fig. 8(a). As with the area, the shape of the weld pool is mainly a function of the heat input, and as mentioned above, once the weld pool is established in its quasi-stationary zone, it should maintain a constant shape. Nevertheless, in Fig. 8(b), fluctuations of the features appear due to the weld pool dynamics and convective exchanges, and the filler metal also intervenes in the modification of the energy distribution within the weld pool. Furthermore, the ends of the melt across the width compared to fixed data on the image such as the tungsten position, which is fixed due to a fusion line. Fig. 8(b) shows the area of the weld pool, its width, and one end of weld pool with regard to the position of the tungsten. Monitoring this characteristic (DistXmin - Posi W) allows us to observe

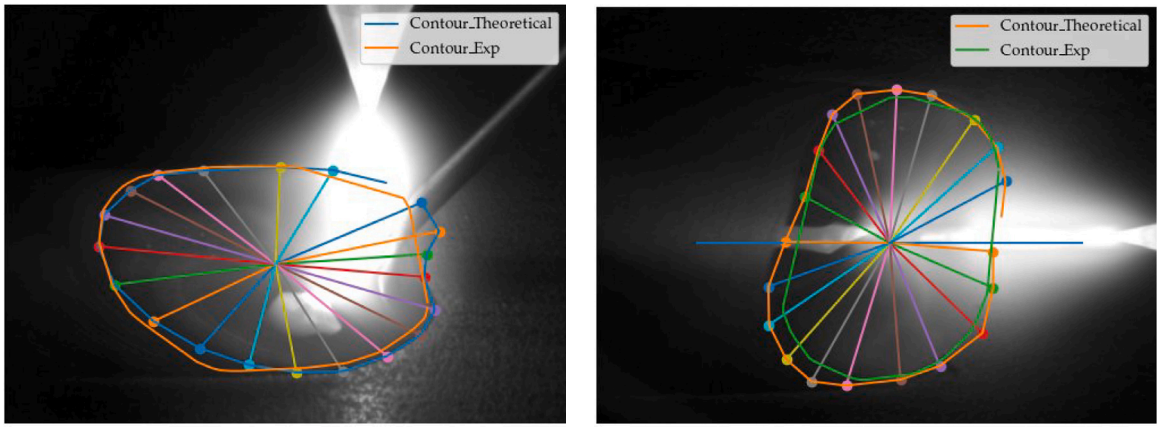

Fig. 10. Weld pool contour comparison: experimental vs theoretical measurement (manual). (a) Side view. (b) Top view.

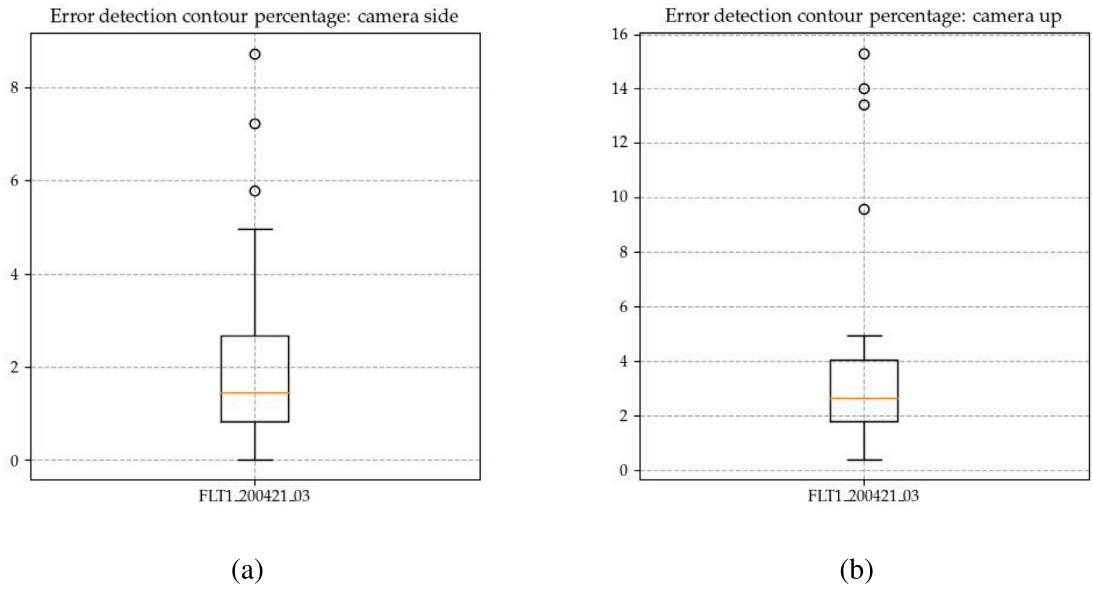

Fig. 11. Percentage weld-pool contour detection error of all experimental contours vs theoretical measurement (manual). (a) Side view. (b) Top view.

the phenomenon of instability (excessive oscillation) while keeping the area and a bounding box constant.

Measurement error on contour detection

As mentioned above, the presence of the electric arc during welding, being extremely radiant, induces multiple disturbances of electrostatic, electromagnetic, thermal, and visual nature. Particular attention must be paid to the extreme luminosity, which is a source of significant disturbance when it comes to visualizing the weld pool. Fig. 9 presents the edge detection error per field of view for the experiment analyzed in Section "Experiment analysis". The results show a detection of contours of higher than 90% during the experiment, which is satisfactory considering the required constraints.

In addition, other sources of error may be present in the detection of contours such as the presence of oxide on the weld-pool surface and filler metal dynamics. Finally, the curved nature of the weld pool also leads to errors in detection of the contours as it leads to darker shades of gray on the weld pool ends, which the algorithm struggles to take into account.

Fig. 10 shows an example of experimentally calculated contours compared to melt-pool contours recovered by hand from the image (theoretically). This contour was then compared to the algorithm result to extract the weld-pool geometry. The theoretical calculation of the weld-pool contours was supervised by the same person who manually retrieved the contours in order to avoid sources of error in the interpretation of the area of interest. From the theoretically calculated contour centroid, the radius as a function of the angle (at each point in the weld pool contour) was calculated on the melt delimitation. In addition, this action was performed on the experimental contour to calculate the percentage uncertainty of the radius versus angle as shown in Fig. 11.

In general, less than a 10% difference is found on the radius between manual versus automatic contour recovery. However, some points around the weld pool may fall outside this range, resulting in an uncertainty of up to 18%. These points are mainly located at the bottom of the back side of the bead because of the curved bead aspect.

Specific database for machine learning

In order to test our ML algorithms on experimental data, allowing us to predict or classify the welding procedure specifications (WPS), a new database of weld-pool characteristics is required (Section "Extraction of weld-pool image features"). On the one hand, this allowed a reduction of the former database of raw data (raw images, replaced by the

Table 2
GTAW welding process parameters.

Experiment	Intensity (A)	Voltage (V)	Welding speed (m/min)	E (J/mm)	Wire feed rate (m/min)	Gas flow rate (L/min)
FLT1_200421_01	100	9.7	0.07	831.4	1.2	11.5
FLT1_200421_02	120	10.4	0.08	936	2.0	11.5
FLT1_200421_03	150	11.8	0.15	708	3.0	13.0
FLT1_200421_04	180	11.9	0.15	856.8	3.0	13.0

respective geometrical weld-pool characteristics). On the other hand, this helps to speed up the processes of training, testing, and validation of the various ML algorithms used.

The parameters used in these tests are shown in Table 2. These four welding procedure specifications (FLT1 = Fusion Line TIG 1, cf. Section "Data structure and traceability") allow the development of a multi-physics database (multi-sensors as presented in Section "Materials and methods") that feeds data from the learning and testing phase to ML algorithms.

Machine learning for welding

The welding procedure specification is a document detailing the protocol and required variables (process parameters) for the welding operation in order to ensure repeatability once in production. Classification algorithms are of particular interest because they provide a means to verify that the process is being performed under the right conditions. For this reason, different operating modes were used, and a classification algorithm was implemented.

Modeling of KNN-based weld-parameter prediction

Supervised learning

The main aims of this study are to classify the different process parameters, and to test the ML model ability to predict operating mode variation. For the first objective, the performance of a decision algorithm is analyzed; in this case, k-nearest neighbor (KNN). This particular algorithm is a supervised machine-learning algorithm.

[2] present supervised learning and its learning, testing and validation structure. Supervised learning consists in learning the link between two sets of data. In the present study, these data sets are the observed data X (here the geometrical characteristics) and an output variable Y (here the process parameters), which we try to predict (2). The data are labeled not by their reference (Section "Data structure and traceability") but by the acronym used to identify the experiment run and the intensity (in A) programmed for that particular welding operation. For example, FLT1_200421_01 (cf. Table 2), welded with a current of 100 A becomes FLT1_100 A.

$$Y = f(X) \tag{2}$$

.

In the proposed method, the prediction of process parameters such as intensity (FLT1_100 A, FLT1_120 A, FLT1_150 A, FLT1_180 A) is divided into three phases. Fig. 12(a) illustrates the different learning steps. First, the weld-pool geometrical characteristics data are processed and stored as training data. Here, the training set is used to train the algorithm and to adjust the model parameters used, while the test set is necessary to verify the resulting performance and to measure the prediction error in order to choose between several model parameter configurations. Second, the data are divided into random training and test subsets. The validation dataset is later used for validation of the KNN algorithm. This guarantees the robustness of the algorithm. Furthermore, to increase the model performance, cross-validation is used (Fig. 12(b)). The principle of this method is to randomly partition the training and test data into n subsets. This process is repeated n times so that each subset is used for the training and test phase. The average cross-validation error is used as a performance indicator.

Table 3
K-nearest neighbor algorithm.

Nearest-neighbor algorithm
1: Define k
2: **while** (the stopping criterion is not respected) **do**
3: → Calculate the distance to other data points
4: → Sort the calculation distances
5: → Select the k-point at the shortest distance
6: → Assign the test point to the class that has the most points in its environment
7: –> Return the selected class
8: **end while**

KNN process

Various classification algorithms have been used in the study of classifying data. These include tree decision methods, random forest, naïve Bayes, support vector machine, and nearest neighbor methods [2]. The k-nearest neighbor (KNN) algorithm is a supervised learning classification technique. The algorithm works based on intuition (nonparametric method). The closest points are more likely to belong to the same class. When a new point is introduced, it is added to the majority class of its nearest neighbor.

The kNN algorithm steps can be represented as follows (see Table 3)
:

Each ML model has hyperparameters specific to the algorithm used. A hyperparameter is a parameter that is defined before the learning process begins. A method exists for hyperparameter optimization: the exhaustive grid search technique. This takes and tries all the desired hyperparameter combinations in order to find the best combination. However, this can take time and requires computational resources for each additional parameter value.

For the K-nearest neighbor algorithm, three hyperparameters can be tested and used, n-neighbors, weight, and metric. Here, the n-neighbors hyperparameter decides the best k-nearest neighbor. The weight checks whether or not adding weights to data points is beneficial; there are two different weights: "uniform" which assigns no weight, and "distance" which weights the points by the inverse of their distances, which means that the closest points will have more weight than the farthest points. Finally, the last hyperparameter is the distance metric, which calculates the similarity (observation more likely to be the same class). There are three different versions of this hyperparameter: "Minkowski", "euclidean", and "manhattan".

Evaluation criteria

The quantification of model performance is based on various metrics: classification, "classification report", "validation curve", and many others. A "classification report" is used to measure the quality of predictions from a classification algorithm. The report shows the main classification metrics, namely "precision", "recall", and "f1-score", on a per-class basis. These metrics are calculated from true positives, false positives, true negatives, and false negatives. In addition, one of the most commonly used is classification accuracy, which is the number ratio of correct predictions to the total number of input samples. Furthermore, it can be interesting to analyze the learning curve in order to identify the model performance as a function of the number of samples in the learning base.

Fig. 12. (a) Data structure for ML. (b) Cross validation example: randomly partition the training and test data into *n* subsets.

Table 4
Dataset split between training, test, and validation for a four-class test : Side camera.

Category	Train	Test	Validation
FLT1-100	8791	2198	3690
FLT1-120	7542	1886	3177
FLT1-150	3503	876	1450
FLT1-180	3500	875	1443
Total	23336	5835	9760

Table 5
Dataset split between training, test, and validation for a four-class test : Top camera.

Category	Train	Test	Validation
FLT1-100	8744	2186	3665
FLT1-120	7567	1892	3124
FLT1-150	3355	839	1414
FLT1-180	3335	834	1454
Total	23001	5751	9657

Data structure

The aim of the tests is to obtain nondefective welds that are representative of the weld conditions. The melt contour dataset is a classification task consisting of identifying four types of intensities from geometric features. The data set consists of approximately 39000 images from 12 weld beads (three operating modes per configuration, each with a different feed rate, whilst keeping a similar deposited bead length (100 mm). The number of images differs between the runs because the welding times are different and the camera records have the same frequency. Tables 4 and 5 describe the dataset composition used for the two studied view points (top and side camera).

Finally, a validation database is made including one operating mode per configuration to study the machine learning model performance used. The algorithm used, here KNN, must classify each welding procedure specification in its respective class. Although a particular parameter may not be sufficient to predict whether or not a weld will meet specifications, it may allow us to validate or discard our choice of ML model.

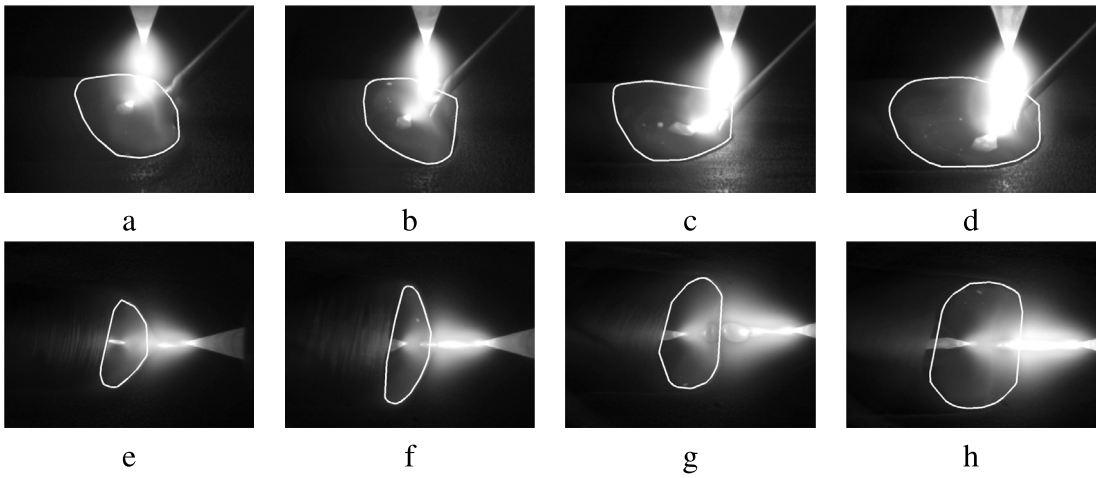

Fig. 13. Visualization of weld-pool contours for different current intensities, in the two fields of view. First row: Side view. Second row: Top view. Panels (a) and (e): intensity = 100 A; Panels (b) and (f): 120 A; Panels (c) and (g): 150 A; Panels (d) and (h): 180 A.

Results and discussion

In this section, the weld-pool behavior during a TIG welding operation is discussed for the four operating modes. Then, the classification of the parameter data using the ML algorithm is presented.

Influence of current intensity on weld-pool dimensions

After processing the images obtained through the methods presented above, the contours of the weld pool were acquired. Fig. 13 shows the contours for each configuration and in both fields of view (Side view: panels (a to d); top view: panels (e to h). Subsequently, different quantities, such as length, width, and area of the weld pool, among others, were extracted (see Section "Extraction of weld-pool image features").

To study the influence of current intensity on the weld-pool dimensions, the dimensions of the weld pool with the different configurations were carefully measured in a quasi-stationary state. Fig. 14 shows a comparison of the areas over time in the quasi-stationary zone, that is, between the end of the initiation phase and the arc-extinction phase for the two fields of view. Fig. 14 shows that an increase in welding current leads to an increase in the area of the weld pool in top view (same result for side view). The impact of current intensity on the weld-pool geometry is seen even more clearly from the images in Fig. 13. Furthermore, the current is not the only parameter that influences the weld-pool dimensions. The wire feed rate, the tension, and the welding speed will also influence the heat distribution due to convection forces.

The analysis of Fig. 14 reveals repeatability between the same trials of any chosen parameter configuration. In addition, the melt-pool dimensions increase with power (UI) in both fields of view. Fig. 14 reveals that heat input is not the only criterion to take into consideration when characterizing the weld-pool dimensions; wire speed rate is also to be taken into account. For the run WPS FLT_120, which has the highest heat input, weld-pool area is lower than WPS FLT_150 because the material input per unit of time is higher.

Comparison of weld-pool features with classification KNN algorithms

Weld-pool feature database for ML

In this paper, different geometric features, such as bounding box (width and length), area, and other features, extracted using image processing algorithms, are presented,as illustrated in Fig. 15. Access to these quantities allow us to deduce information about the weld-pool stability over time and the repeatability of the welding process. In addition, contour extraction allows us to follow variations in the weld-pool geometry as a function of heat input or current intensity (see Section "Influence of current intensity on weld-pool dimensions").

In this section, the ability of the ML algorithm to classify and then predict the operating modes from experimental data is tested. To do this, a new database is implemented from the weld-pool geometry, allowing reduction of the data, ultimately saving time when training the different ML algorithms tested.

Table 6
Detailed classification report for each class in the database. Side-on camera field of view.

Detailed classification report			
Category	Precision	Recall	F1-score
FLT1-100	1.0	1.0	1.0
FLT1-120	1.0	1.0	1.0
FLT1-150	1.0	1.0	1.0
FLT1-180	1.0	1.0	1.0
Accuracy			1.0

Table 7
Detailed classification report for each class in the database. Top camera field of view.

Detailed classification report			
Category	Precision	Recall	F1-score
FLT1-100	1.0	1.0	1.0
FLT1-120	1.0	1.0	1.0
FLT1-150	1.0	1.0	1.0
FLT1-180	1.0	1.0	1.0
Accuracy			1.0

Classification report

Tables 6 and 7 show precision, recall, and macro F-score for the models trained and tested on the two fields of view (side and top), respectively. Out of all the labels to be predicted, the algorithm manages to classify each sample (test subset) into its correct label (class : FLT1_100, FLT1_120, FLT1_150, or FLT1_180). Moreover, the computation time for this method is about 0.80 s.

The model KNN shows a good classification performance on these data because, on the one hand, as shown in Fig. 14, weld-pool area over time can be seen to be similar in runs with the same parameter configuration and the groups of runs can be separated according to weld-pool area, which appears to correlate well with current intensity. On the other hand, as shown in Fig. 13, the change in weld-pool geometry is visible to the naked eye. Furthermore, the model performance mainly depends on clarity and sharpness of the data injected into the model.

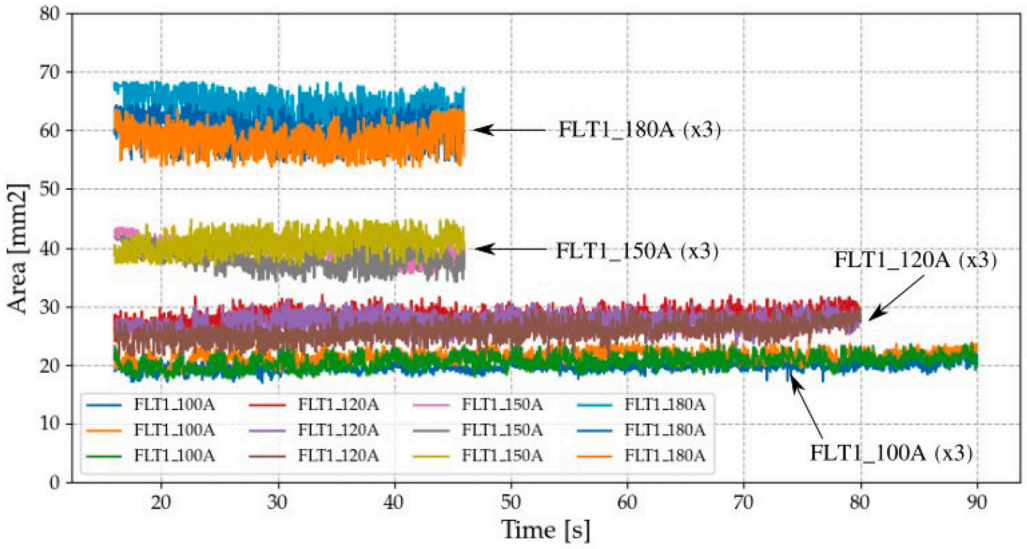

Fig. 14. Evolution of areas over time for different current intensities (100 A, 120 A, 150 A, 180 A); top view.

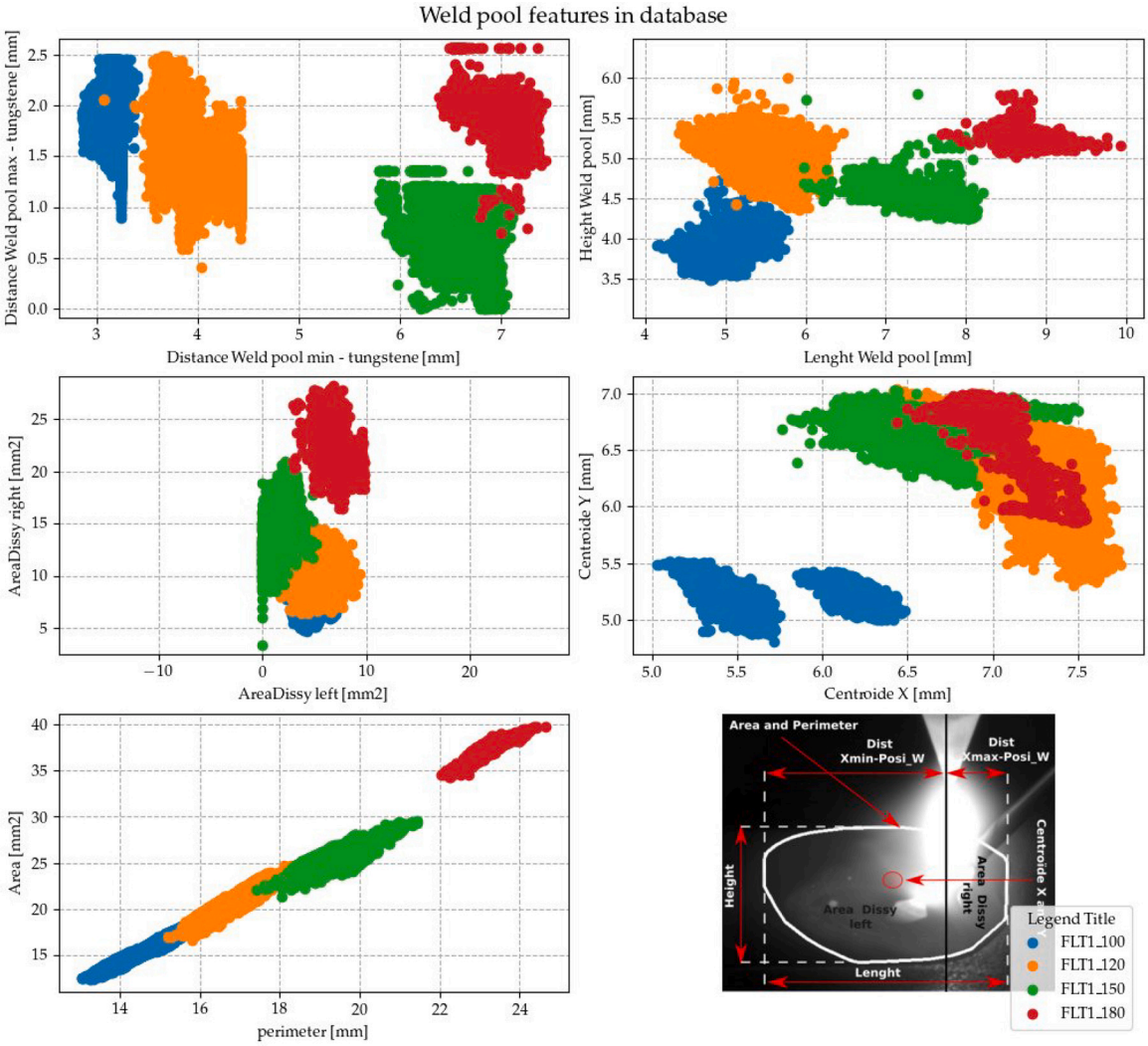

Fig. 15. Features characteristic extract from a weld pool contour.

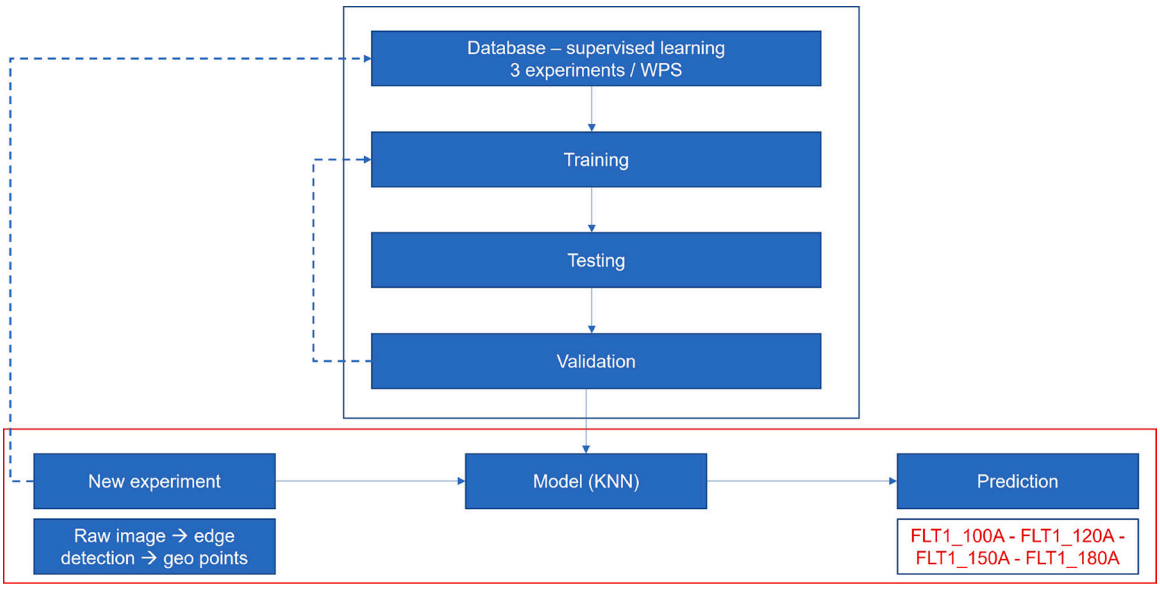

Fig. 16. Prediction structure for machine learning.

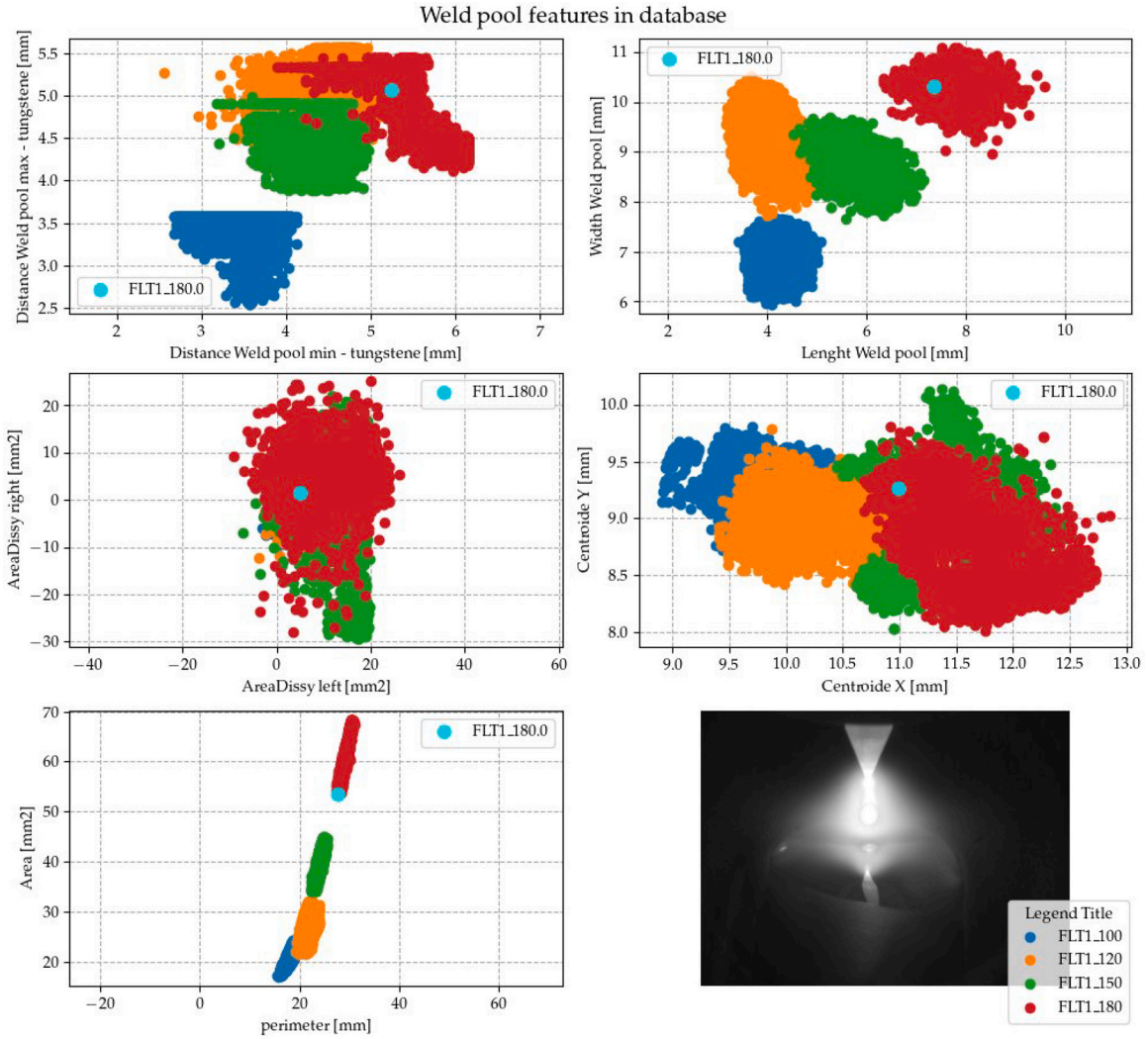

Fig. 17. Extraction of characteristic features of a weld-pool contour and prediction of a contour by the algorithm.

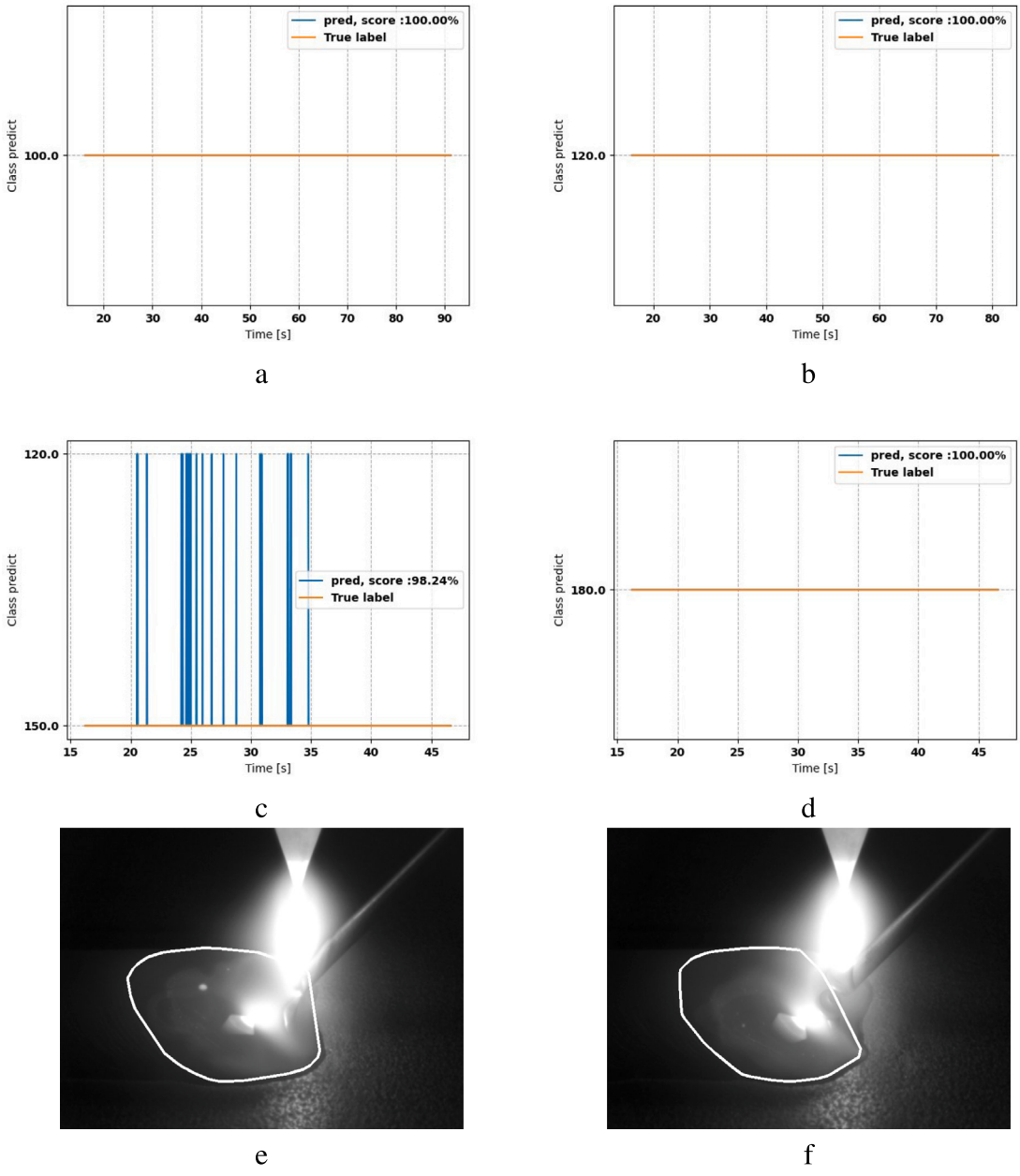

Fig. 18. Algorithm prediction results based on images of the weld-pool captured from the side, for different parameter configurations (in this case, different current intensities). Panels: (a) validation experiment FLT_100 A; (b) FLT_120 A; (c) FLT_150 A; (d) FLT_180 A; (e) weld pool detection contour by the algorithm; (f) weld pool fluctuation due to obstruction by dynamic filler metal.

Prediction of current intensity from experimental data with KNN algorithms

Now that the performance quantification of the chosen model (here KNN) has been validated from the different metric results presented above, the next objective is to quantify the ML model performance on new data that were not used to train the model. To do this, a series of new experiments per welding operation class is performed (FLT1_100, FLT1_120, FLT1_150, or FLT1_180). Fig. 16 presents the structure of the prediction algorithm and the steps of the prediction based on an image or a set of images. In the first step, the image is fed into the image-processing algorithm to extract the weld-pool contour. In a second step, the geometric features are extracted. Finally, the data obtained from observations are integrated into the chosen model (here KNN) allowing us to predict the welding operation class : FLT1_100, FLT1_120, FLT1_150, or FLT1_180.

Fig. 17 presents an example of a prediction point result for an experimental welding run performed with an intensity of 180 A. The image presented was captured by top view camera. All of the different features are represented, such as the area, the centroids, the bounding box, and so. The data points are color-coded according to class, as shown in the key in the bottom right corner of the figure. The turquoise point shown in each of the panels of Fig. 17 is the algorithms prediction for each weld-pool feature based on the input data. The point is consistently placed by the algorithm into the right point cloud (FLT_180), which corresponds to the right programmed intensity. The classification algorithm has predicted the right class from the input data for weld-pool geometry.

Fig. 18 shows the algorithm prediction results for an FLT welding run based on data obtained from an image of the weld pool captured from the side. In panels (a), (b), and (d), the prediction result for the contours is 100% for accuracy score, and in figure (c), the prediction made by the algorithm for the FLT_150 experiment is 98.24%, which is a very good performance. Moreover, as the time point at which each

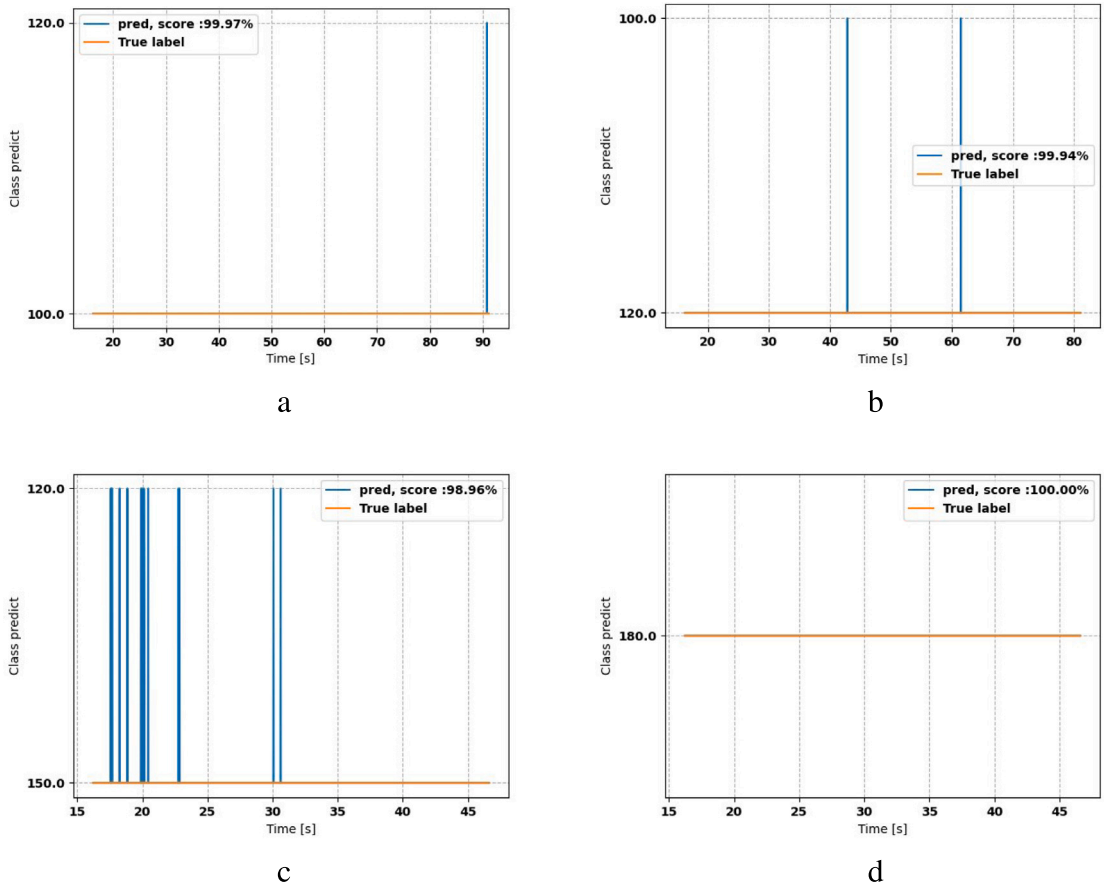

Fig. 19. Algorithm prediction results based on images of the weld-pool captured from the side, for different parameter configurations (in this case, different current intensities). Panels: (a) validation experiment FLT_100 A; (b) FLT_120 A; (c) FLT_150 A; (d) FLT_180 A.

image was captured during the welding run is know, it is possible to display the contour prediction results superimposed on the image in question. By analyzing the images for which the prediction is different from the true label, we can see that this discrepancy is due to measurement errors caused by the filler metal drip; its appearance in the field of view of the camera results in variation of the contour detected by the algorithm (Fig. 18(f)).

Fig. 19 shows prediction results for each welding procedure specification based on images of the weld pool as seen from above (top camera view) during the quasi-stationary welding phase. The results also show a prediction of over 98% of good class detection. The analysis on the "bad" prediction also shows the same conclusions as before. This is due to measurement errors related to the weld-pool dynamics.

Conclusions and perspectives

This study has effectively devised an experimental configuration and protocol for conducting in-situ analysis and monitoring of the TIG welding process. The use of cameras and sensors facilitated ongoing monitoring and regulation of significant welding parameters, including voltage, intensity, shielding gas, and wire feed rate. The challenges of measuring radiation from the arc were resolved through the use of specific filters. This allowed for accurate image capture of the weld pool without requiring any external lighting.

The efficient use of machine learning models is facilitated by the creation of a comprehensive database, enriched with information on weld pool geometry and variations in process parameters over time. This new data reduces the database size and the time needed for training/testing ML models. After training, these models showed a strong predictive ability for welding parameters, particularly current intensity, based on images of the weld pool. The potential for real-time process control and refinement of welding procedures is highlighted by the performance of these models.

However, it should be noted that the accuracy of the contour detection algorithm played a key role in the performance of the model and may be affected by disturbances arising from filler metal input and arc radiation. These issues will be addressed and minimized in future investigations, thereby increasing the robustness of the approach.

Further research should investigate diverse classification models for predicting welding operation quality and compare their performances. Moreover, the inclusion of deep learning techniques like convolutional neural networks (CNNs) could offer more advanced abilities for image analysis and process monitoring. Comparing different criteria for assessing the predictive capacities of machine learning and deep learning algorithms will enhance the refinement of these techniques.

Moreover, future work may involve applying these algorithms to more complex welding configuration that are representative of manufacturing operations, including multi-pass filling and intricate geometries. These configuration can reveal critical defects and changes in wettability, contributing to improved quality control and efficiency in the welding industry. Overall, this study paves the way for innovative advancements in welding process control and quality assurance through the integration of modern techniques based on experimental data and machine learning.

CRediT authorship contribution statement

Theo Boutin: Conceptualization (lead), Data curation (lead), Formal analysis (lead), Investigation (lead), Methodology (lead), Software (lead), Supervision (lead), Project administration (lead), Validation

(lead), Visualization (lead), Writing – original draft (lead), Writing – review (lead). **Issam Bendaoud:** Conceptualization (supporting), Data curation (supporting), Formal analysis (supporting), Investigation (supporting), Methodology (supporting), Software (supporting), Validation (supporting), Visualization (supporting), Writing – review (supporting). **Josselin Delmas:** Project administration (lead), Funding acquisition (lead), Resources (lead), Supervision (supporting), Conceptualization (supporting), Data curation (supporting), Formal analysis (supporting), Investigation (supporting), Methodology (supporting), Software (supporting), Validation (supporting), Visualization (supporting), Writing – review (supporting). **Damien Borel:** Conceptualization (supporting), Data curation (supporting), Formal analysis (supporting), Investigation (supporting), Methodology (supporting), Software (supporting), Validation (supporting), Visualization (supporting), Writing – review (supporting). **Cyril Bordreuil:** Supervision (lead), Project administration (equal), Resources (supporting), Conceptualization (supporting), Data curation (supporting), Formal analysis (supporting), Investigation (supporting), Methodology (supporting), Software (supporting), Validation (supporting), Visualization (supporting), Writing – review (supporting), Writing – original draft (supporting).

Declaration of competing interest

The authors declare that they have no known competing financial interests or personal relationships that could have appeared to influence the work reported in this paper.

Acknowledgments

The authors would like to acknowledge the financial support of the Agence Nationale de la Recherche and Électricité de France.

Supplementary data

Supplementary material related to this article can be found online at https://doi.org/10.1016/j.cirpj.2023.09.006.

References

[1] D. Bacioiu, G. Melton, M. Papaelias, R. Shaw, Automated defect classification of aluminium 5083 TIG welding using HDR camera and neural networks, J. Manuf. Process. 45 (June) (2019) 603–613, http://dx.doi.org/10.1016/j.jmapro.2019.07.020.

[2] T. Dietterich, C. Bishop, D. Heckerman, M. Jordan, M. Kearns, Associate Editors, Adaptive Computation and Machine Learning, 2022.

[3] R. Duda, P. Hart, D. Stork, Pattern classification (z-lib.org).pdf, 2000.

[4] M.A. Ezer, G. Çam, A study on microstructure and mechanical performance of gas metal arc welded AISI 304 L joints, Mater.wiss. Werkst.tech. 53 (9) (2022) 1043–1052, http://dx.doi.org/10.1002/mawe.202200050.

[5] M. Grasso, F. Gallina, B. Colosimo, Data fusion methods for statistical process monitoring and quality characterization in metal additive manufacturing, Procedia CIRP 75 (2018) 103–107, http://dx.doi.org/10.1016/j.procir.2018.04.045.

[6] M. Khanzadeh, S. Chowdhury, M. Marufuzzaman, M. Tschopp, Bian, Porosity prediction: Supervised-learning of thermal history for direct laser deposition, J. Manuf. Syst. 47 (662) (2018) 69–82, http://dx.doi.org/10.1016/j.jmsy.2018.04.001.

[7] C. Knaak, G. Kolter, F. Schulze, M. Kröger, P. Abels, Deep learning-based semantic segmentation for in-process monitoring in laser welding applications, 1113905 (September), 2019, p. 2, http://dx.doi.org/10.1117/12.2529160.

[8] R. Kovacevic, Zhang, Real-time image processing for monitoring of free weld pool surface, Trans. ASME, J. Manuf. Sci. Eng. 119 (2) (1997) 161–169, http://dx.doi.org/10.1115/1.2831091.

[9] J. Lancaster, The Physics of Welding, 1986, http://dx.doi.org/10.1016/c2013-0-03805-4,

[10] R.W. Messler, Principles of Welding: Processes, Physics, Chemistry, and Metallurgy, 1999.

[11] J. Mirapeix, P. García-Allende, A. Cobo, O. Conde, J. López-Higuera, Real-time arc-welding defect detection and classification with principal component analysis and artificial neural networks, NDT E Int. 40 (4) (2007) 315–323, http://dx.doi.org/10.1016/j.ndteint.2006.12.001.

[12] J. Mirapeix, R. Ruiz-Lombera, J. Valdiande, L. Rodriguez-Cobo, F. Anabitarte, A. Cobo, Defect detection with CCD-spectrometer and photodiode-based arc-welding monitoring systems, J. Mater Process. Technol. 211 (12) (2011) 2132–2139, http://dx.doi.org/10.1016/j.jmatprotec.2011.07.011.

[13] M. Senol, G. Cam, Investigation into microstructures and properties of AISI 430 ferritic steel butt joints fabricated by GMAW, Int. J. Press. Vessels Pip. 202 (January) (2023) 104926, http://dx.doi.org/10.1016/j.ijpvp.2023.104926.

[14] H.T. Serindag, G. Çam, Characterizations of microstructure and properties of dissimilar aisi 316l/9Ni low-alloy cryogenic steel joints fabricated by gas tungsten arc welding, J. Mater. Eng. Perform. 32 (August) (2022) 7039–7049, http://dx.doi.org/10.1007/s11665-022-07601-x.

[15] H.T. Serindag, G. Çam, Multi-pass butt welding of thick AISI 316l plates by gas tungsten arc welding: Microstructural and mechanical characterization, Int. J. Press. Vessels Pip. 200 (October) (2022) 104842, http://dx.doi.org/10.1016/j.ijpvp.2022.104842.

[16] H. Serindag, C. Tardu, İ. Kircicek, G. Cam, A study on microstructural and mechanical properties of gas tungsten arc welded thick cryogenic 9, CIRP J. Manuf. Sci. Technol. 37 (2022) 1–10, http://dx.doi.org/10.1016/j.cirpj.2021.12.006.

[17] A. Sumesh, B. Nair, K. Rameshkumar, A. Santhakumari, A. Raja, K. Mohandas, Decision tree based weld defect classification using current and voltage signatures in GMAW process, Mater. Today Proc. 5 (2) (2018) 8354–8363, http://dx.doi.org/10.1016/j.matpr.2017.11.528.

[18] A. Sumesh, K. Rameshkumar, K. Mohandas, R. Shyam-Babu, Use of machine learning algorithms for weld quality monitoring using acoustic signature, Procedia Comput. Sci. 50 (2015) 316–322, http://dx.doi.org/10.1016/j.procs.2015.04.042.

[19] A. Sumesh, D. Thekkuden, B. Nair, K. Rameshkumar, K. Mohandas, Acoustic signature based weld quality monitoring for SMAW process using data mining algorithms, Appl. Mech. Mater. 813–814 (2015) 1104–1113, http://dx.doi.org/10.4028/www.scientific.net/amm.813-814.1104.

[20] M. Systems, Field wiring and noise considerations for analog signals, (April 1992), 2014, pp. 1–12.

[21] S. Verma, M. Gupta, J. Misra-Prakash, Performance evaluation of friction stir welding using machine learning approaches, MethodsX 5 (May) (2018) 1048–1058, http://dx.doi.org/10.1016/j.mex.2018.09.002.

[22] D. You, X. Gao, S. Katayama, WPD-pca-based laser welding process monitoring and defects diagnosis by using FNN and SVM, IEEE Trans. Ind. Electron. 62 (1) (2015) 628–636, http://dx.doi.org/10.1109/TIE.2014.2319216.

[23] Y.M. Zhang, R. Kovacevic, Neurofuzzy model-based predictive control of weld fusion zone geometry, IEEE Trans. Fuzzy Syst. 6 (3) (1998) 389–401, http://dx.doi.org/10.1109/91.705507.